



# Optimization of the Power Coefficient of a Savonius Wind Turbine by Changing the Shape of Blades

Medhat E. M. Abu Khers<sup>a</sup>, Mahmoud Fouad<sup>b</sup>, Taher Halawa<sup>c</sup>

<sup>a</sup> R&D Department, Aircraft Factory - Arab Organization for Industrialization (AOI), Helwan, Egypt.

<sup>b</sup> Professor, Mechanical Power Engineering Department, Cairo University, Giza, Egypt.

<sup>c</sup> Associate Professor, Mechanical Power Engineering Department, Cairo University, Giza, Egypt.  
Mechanical Engineering Department, British University in Egypt (BUE), Al-Sherouk City, Egypt.

**Abstract :** There is a growing necessity to increase the efficiency of wind turbines especially the vertical axis type. One of the challenges is to enhance the performance of Savonius wind turbines. Several methods have been used for improving the power extraction efficiency through making some modifications in the shape of blades. There is an important raised question about the best shape of blades that will maximize the power coefficient of the Savonius wind turbine. This paper tries to answer this question by introducing an optimization analysis using the optimal control numerical approach. Results indicated that the most important part of the blade that influences the turbine efficiency is close to the tip radius of the blades. The combined effect of making gradual slope of the blade profile and directing the blade curvature to be slightly outward near the tip region was impressive. The flow separation point was shifted. The pressure distribution on blades surfaces was improved and thus, the torque was increased. The third proposed design achieves an increase of 71% in the value of the power coefficient corresponding to a free stream wind speed of 6 m/s compared to the conventional semi-circle design.

**KEYWORDS :** CFD, Savonius style wind turbine; Power coefficient; Torque coefficient; Tip speed ratio.

## Nomenclature

$A$	Swept area of the turbine (m <sup>2</sup> )	$\bar{\omega}$	Flow field variable
$A_j$	Area vector [m <sup>2</sup> ]	$\zeta$	Physical boundary location
$C_p$	Power coefficient	$\psi$	Lagrange Multiplier factor
$C_T$	Torque coefficient	$\phi$	Symbol for general flow variable
$d$	Chord length of the blades (m)	$\rho$	Fluid density [Kg/m <sup>3</sup> ]
$D$	Outer diameter of the turbine (m)	$\Gamma$	Diffusion coefficient
$D_0$	End plate diameter (m)	$\nabla$	The gradient of a value
$G$	Gradient of the desired cost function	$\omega$	Rotational speed of the turbine (rad/s)
$H$	Height of the turbine (m)	$\theta$	Turbine angle to the wind direction (°)
$I$	Objective function	$\lambda$	Tip speed ratio
$n_f$	Number of faces on the control volume	$\nu$	Kinematic viscosity of the fluid (m <sup>2</sup> /s)
$R$	Radius of rotation of the turbine (m)	$\Delta t$	Time step [s]
$Re$	Reynolds number	$\delta t$	Incremental change in time [s]
$S$	Flow solution	$\delta V$	Incremental change in mesh volume [m <sup>3</sup> ]
$S^\phi$	The source term of $\phi$	$V_w$	Free stream wind speed (m/s)
$T$	Time [s]	$V$	Mesh volume [m <sup>3</sup> ]
$T$	Dynamic torque on the turbine (N.m.)	$u^s$	Mesh velocity of the moving mesh [m/s]
$y^+$	Dimensionless wall distance	$u$	Flow velocity vector [m/s]

## Abbreviations

CFD	Computational fluid dynamics
HAWTs	Horizontal axis wind turbines
URANS	Unsteady Reynolds-Averaged Navier–Stokes equations
VAWTs	Vertical axis wind turbines

## Introduction

The growth rate of using wind energy to generate power is increasing day after day. Generally, the efficiency of power extraction from wind is higher for horizontal axis wind turbines (HAWTs) than for vertical axis wind turbines (VAWTs). However, recently great developments occurred in the research related to increasing the efficiency of VAWTs. In some situations, VAWTs have more advantages than HAWTs, including being independent on wind direction, ease of maintenance, simple design, less noise pollution, and acceptable power generation under low wind speed conditions. These advantages in parallel with the significant recent developments expand the usage of VAWTs and increase the necessity of improving their performance to obtain a high total power output.

The two main configurations of VAWTs are Savonius and Darrieus [1]. The Savonius rotor model was developed by Sigurd Johannes Savonius in 1929 [2]. The concept of the Savonius turbine is based on extracting the wind energy by the drag force.

Many researchers studied the optimization of the Savonius wind turbine using various approaches including changing the number of blades, modifying the aspect ratio, increasing the number of stages, adding deflector in front of the turbine, changing the overlap and spacing of buckets and changing the shape of blades and their thickness (Fig.1).

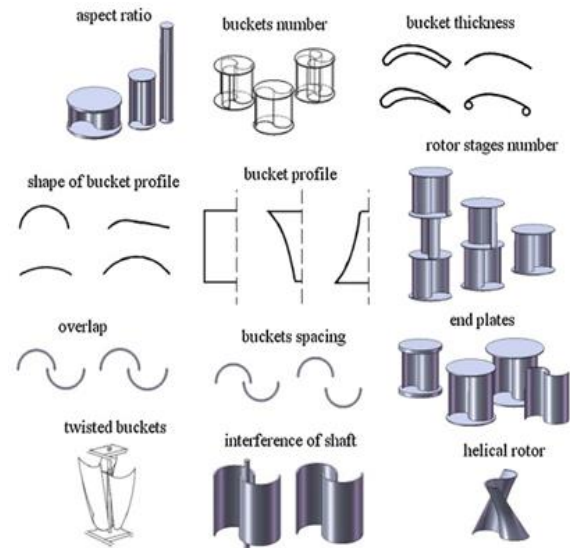


**FIG 1.** Most common parameters studied by researchers to optimize the efficiency of the Savonius wind turbine [3]

Hassanzadeh et al. [4] studied the effect of changing the blade diameter to depth ratio for a two blade conventional Savonius turbine at different tip speed ratios and wind speeds. Based on the presented results, it was found that the maximum power coefficient occurred for the design with a blade diameter to depth ratio of 0.5. Saha et al. [5] studied the effect of twisting the rotor blades on the power coefficient. It was found that the twist angle of 15 degrees achieves the optimum power coefficient. The power coefficient was found to be increased when the twist angle of the rotor is 45 degrees at specific conditions [6,7]. El-Askary et al. [8] noted that increasing the aspect ratio to be more than 2 leads to an increase in the peak values of torque and power coefficients for a twisted rotor. Zhang et al. [9] introduced a blade shape optimization analysis using a novel wake energy method. The power coefficient of an optimized ARC-Blade Savonius wind turbine was higher than that for the classical shape of Savonius wind turbine by 10.98%.

Gad et al. [10] used parabolic equations to develop design of Savonius wind turbine that

increase the power coefficient. Using elliptical blades can increase the lift and drag coefficients compared to semi-circle blades in addition to enhancing the performance with an improvement that can reach to 20.25% [11]. Kacprzak, Liskiewicz, and Sobczak [12] indicated that the semi-elliptic blade profile provides better efficiency than the semi-circle, and Bach profile types when the tip speed ratio is within the range from 0.2 to 0.4. Alom and Saha [13] noted that the power coefficient peak value of a Savonius turbine with a semicircle blades can be increased from 0.272 to 0.304 when using elliptical blades and to 0.34 when using a specific modified Bach type rotor. Roy and Saha [14] investigated experimentally different blade profiles for a Savonius wind turbine. Results showed that a newly developed profile achieved increase in the torque coefficient by 4.2%, 11.1%, 22%, and 31.6% comparing with the Bach type, Benesh blade, semi-elliptic, and semi-circle profiles, respectively. Roy and Ducoin [15] made a modification to the blade of Savonius turbine and compared its efficiency with a conventional semi-circle turbine. It was shown that for all tip speed ratios, the turbine with modified blade improved the power compared to the conventional turbine. Ramadan et al. [16] reported a significant increase in the value of the maximum power coefficient (about 64.7 %) when using a specific S-shape profile of a two blade Savonius wind turbine compared with the turbine with conventional blades when the wind speed is 9 m/s. Tartuferi et al. [17] introduced an innovative design of Savonius turbine by using blades with the shape of airfoil. When the value of the tip speed ratio is lower than 0.5 and higher than 0.9, the performance of the innovative turbine design is better than the semicircle blades design. Tian et al. [18] suggested a new design of Savonius rotor based on the modification of both sides of the blades. The maximum power coefficient was found to be higher by 4.41% for the new design compared with the conventional turbine design. Rathod et al. [19] found that the addition of capped vents with various vent ratios to the rotor of a Savonius turbine has negative effect on its performance. The performance of the Savonius turbine was found to be enhances when it is combined with the Darrieus type especially the self-starting characteristics [20]. Saeed, et al. [21] compared four different designs of Savonius rotor blades. One of the proposed designs obtained using optimization numerical analysis provided an enhancement in the power coefficient estimated by 23.9%.

This paper focuses on increasing the power coefficient of a Savonius wind turbine by changing the shape of blades through optimization analysis. The aim is to introduce a novel design that is capable of enhancing the performance of the conventional semi-circle design and to open the way for future studies to make more development of this approach.

## 2. SELECTED WIND TURBINE MODEL

Roy and Saha [14] tested a two-bladed Savonius wind turbine in the wind tunnel shown in Fig. 2. The wind tunnel is composed of five parts which are inlet, diffuser, settling chamber, nozzle, and test sections.

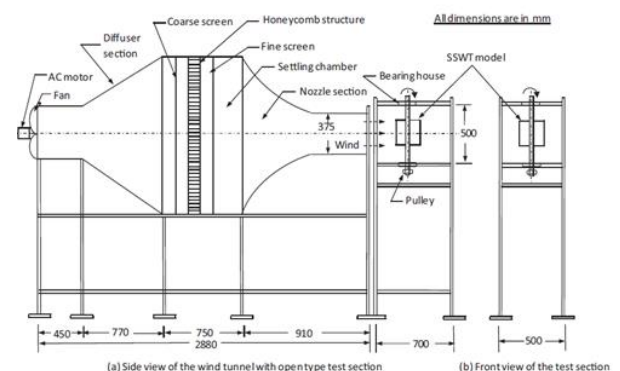


FIG 2. Schematic diagram of the experimental setup [14]

The wind turbine profile selected as the base design in the current presented paper is the conventional semi-circular type (Fig. 3). In this model, the end plates are fixed at the top and bottom sides of the wind turbine for the purpose of improving the pressure difference between the concave and convex surfaces. The diameter of the end plate ( $D_0$ ) is 1.1 times the outer diameter of the turbine ( $D$ ). The thickness of the blades is 0.63 mm. The turbine height ( $H$ ) has the same value as the end plate diameter ( $D_0$ ) and is equal to 230 mm.

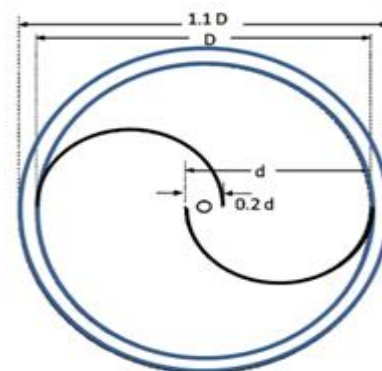


FIG 3. Conventional semi-circular blade profile design tested in the experimental study [14]

### 3. NUMERICAL MODELLING

ANSYS Fluent software [22] was used to make the unsteady numerical simulations by solving the unsteady Reynolds-Averaged Naiver–Stokes equations (URANS). The discretization scheme used for all equations was the second order upwind scheme. The pressure based solver was applied to all numerical models with using the coupled algorithm.

#### 3.1 Modelling of the Wind Turbine Motion

For each numerical model, there are fixed zones and rotating zones. The sliding mesh model was selected to simulate the flow at the interface between the fixed and rotating zones. The following part summarizes the idea of the sliding mesh model theory. The governing equation for a generic variable  $\phi$  according to the sliding mesh model can be written as shown in equation 1.

$$\frac{d}{dt} \int_V \rho \phi dV + \int_{\partial V} \rho \phi (u - u^s) \cdot dA = \int_{\partial V} \Gamma \nabla \phi \cdot dA + \int_V S^\phi dV \quad (1)$$

Where  $V$  is the mesh volume and  $\rho$  is the fluid density. Also,  $u$  and  $u^s$  represent the velocity of the fluid and velocity of the moving mesh respectively.  $\Gamma$  is the coefficient of diffusion and  $S^\phi$  is the source term of the general variable  $\phi$ . The rate of change of the mass with respect to time for second order accuracy flow is described in equation 2.

$$\frac{d}{dt} \int_V \rho \phi dV = \frac{3(\rho \phi V)^{n+1} - 4(\rho \phi V)^n + (\rho \phi V)^{n-1}}{2\Delta t} \quad (2)$$

The index  $n$  represents the existing time step, while the volume at the next time step ( $V^{n+1}$ ) is relate to the time step and the volume at the existing time step as shown in equation 3.

$$V^{n+1} = V^n + \frac{dV}{dt} \Delta t \quad (3)$$

The volume variation rate with respect to time ( $\frac{dV}{dt}$ ) is estimated by taking the sum of dot product of moving mesh velocity vector ( $u_j^s$ ) and the area vector ( $A_j$ ) at each mesh cell face ( $\hat{j}$ ) over the number of faces ( $n_f$ ) as indicated in equation 4.

$$\frac{dV}{dt} = \int_{\partial V} u^s \cdot dA = \sum_j^{n_f} u_j^s \cdot A_j \quad (4)$$

Equation 5 shows how the term  $u_j^s \cdot A_j$  is finally calculated for each control volume.

$$\begin{aligned} (u_j^s \cdot A_j)^{n+1} &= \frac{3}{2} (u_j^s \cdot A_j)^n - \frac{1}{2} (u_j^s \cdot A_j)^{n-1} \\ &= \frac{3}{2} \left( \frac{\delta V_j}{\delta t} \right)^n - \frac{1}{2} \left( \frac{\delta V_j}{\delta t} \right)^{n-1} \end{aligned} \quad (5)$$

Where  $u_j^s \cdot A_j = \frac{\delta V_j}{\delta t}$  is the swept volume by the mesh cell with time.

#### 3.2 Optimization Approach

Regarding the optimization analysis of the wind turbine power coefficient through the modification of the blades profile, there are two main approaches.

The first optimization approach is called gradient based design traditional method. In this method, the objective function is sensitive to each design variable in a way that it is proportional to the number of variables in the design.

On the other hand, the second optimization approach which is known as control theory approach solves separate set of equations to calculate the gradients directly. The method used in the current presented paper is called 'adjoint method' [22, 23] which belongs to the second optimization approach. The advantage of the adjoint method is the independency of its cost on the number of variables in the design. In the adjoint method, the objective function gradient is deduced from the results of an initial simulation with fully converged solution. The objective function ( $I$ ) depends on the flow field variable ( $\bar{\omega}$ ) and the physical boundary location ( $\zeta$ ) as presented in equation 6.

$$I = I(\bar{\omega}, \zeta) \quad (6)$$

Any change occurs in  $\bar{\omega}$  or  $\zeta$  results in formation of  $\delta I$  as expressed in equation 7.

$$\delta I = \frac{\partial I^T}{\partial \bar{\omega}} \delta \bar{\omega} + \frac{\partial I^T}{\partial \zeta} \delta \zeta \quad (7)$$

The flow field which depends on  $\bar{\omega}$  or  $\zeta$  acts as a constraint of the optimization analysis. Equation 8 shows the flow field governing equation.

$$S(\bar{\omega}, \zeta) = 0 \quad (8)$$

The optimization process is limited by the flow and design variables, so this results in having a variation of  $S$  equals to zero (equation 9).

$$\delta S = 0 = \left[ \frac{\partial S}{\partial \bar{\omega}} \right] \delta \bar{\omega} + \left[ \frac{\partial S}{\partial \zeta} \right] \delta \zeta \quad (9)$$

The optimization process is converted from unconstrained type to a constrained one by introducing the Lagrange Multiplier factor ( $\psi$ ) as indicated in equation 10.

$$\delta I = \frac{\partial I^T}{\partial \bar{\omega}} \delta \bar{\omega} + \frac{\partial I^T}{\partial \zeta} \delta \zeta - \psi^T \left\{ \frac{\partial S}{\partial \bar{\omega}} \delta \bar{\omega} + \frac{\partial S}{\partial \zeta} \delta \zeta \right\} = \left\{ \frac{\partial I^T}{\partial \bar{\omega}} - \psi^T \frac{\partial S}{\partial \bar{\omega}} \right\} \delta \bar{\omega} + \left\{ \frac{\partial I^T}{\partial \zeta} - \psi^T \frac{\partial S}{\partial \zeta} \right\} \delta \zeta \quad (10)$$

Equation 11 shows the adjoint equation which was obtained by using  $\psi$  to omit the flow variation terms and producing an explicit formula for the objective function derivative related to design variables only.

$$\left[ \frac{\partial S}{\partial \bar{\omega}} \right]^T \psi = \frac{\partial I}{\partial \bar{\omega}} \quad (11)$$

By inserting equation 11 into equation 10, the relationship between the design variables and the cost function is obtained (equation 12).

$$\delta I = \left\{ \frac{\partial I^T}{\partial \zeta} - \psi^T \frac{\partial S}{\partial \zeta} \right\} \delta \zeta = G^T \delta \zeta \quad (12)$$

Where  $G$  is defined as the cost function desired gradient with respect to the flow solution  $S$  and the design variables.

The solution method is based on having  $\delta I$  with always a negative value while the cost function is minimized during iterative changes [23].

### 3.3 Estimation of Wind Turbine Performance

The performance of a wind turbine can be estimated by evaluating the key parameters, which affect the power output from the turbine. One of these parameters is the tip speed ratio ( $\lambda$ ) which is calculated by dividing the wind turbine tip speed by the free stream wind speed as presented in equation 13.

$$\lambda = \frac{\omega R}{V_w} \quad (13)$$

Where  $\omega$  is the turbine rotational speed, and  $R$  is the turbine tip radius, while  $V_w$  is the wind speed upstream of the turbine.

The power coefficient ( $C_p$ ) is defined as the ratio between the turbine useful power output and the available power in the wind upstream of wind turbine, and is written as shown in equation 14. The torque coefficient ( $C_T$ ) is also indicated in equation 15.

$$C_p = \frac{T\omega}{\frac{1}{2}\rho V_w^3 A} \quad (14)$$

$$C_T = \frac{T}{\frac{1}{2}\rho V_w^2 AR} \quad (15)$$

Equation 16 refers to Reynolds number ( $R_e$ ) which is considered as an important parameter that should be set at different values while monitoring the variation of  $C_p$  and  $C_T$  in order to form a complete view about the turbine performance.

$$R_e = \frac{V_w D}{\nu} \quad (16)$$

Where:  $\nu$  is the kinematic viscosity of air.

Using equations 13, 14, and 15, a relationship between torque and power coefficients and the tip speed ratio can be deduced as clarified in equation 17.

$$C_p = \lambda C_T \quad (17)$$

### 3.4 Computational Grid

The mesh cell shapes selected for generating the mesh were triangles because the triangular mesh element has the ability of modelling complex geometries. The mesh shape is shown in Fig. 4. The dimensionless wall distance ( $y^+$ ) was set to not exceed the value of 0.2. There are 15 inflation layers added at the blades surfaces with a mesh growth rate of 1.2. While creating the mesh, several parameters related to mesh quality were monitored, such as cell aspect ratio and cell skewness. Theoretically, the cell skewness is zero if all triangle cell angles are 60 degrees, so the mesh skewness can be considered a measure of how much is the distortion of the cell with respect to its ideal shape.

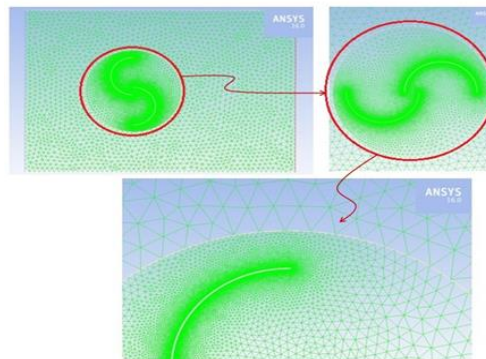


FIG 4. View of the mesh shape in the whole domain and close to blades surfaces

Highly skewed mesh cells should be avoided in the mesh generation process. Furthermore, cell aspect ratio is the ratio between the longest side to the shortest side of the cell and it should be kept close to 1 for high mesh

quality [24]. In the current analysis, the average cell skewness and average cell aspect ratio were 0.1 and 0.9 respectively.

### 3.5 Boundary Conditions

The computational grid is composed of two zones; stationary zone and rotating zone as shown in Fig. 5.

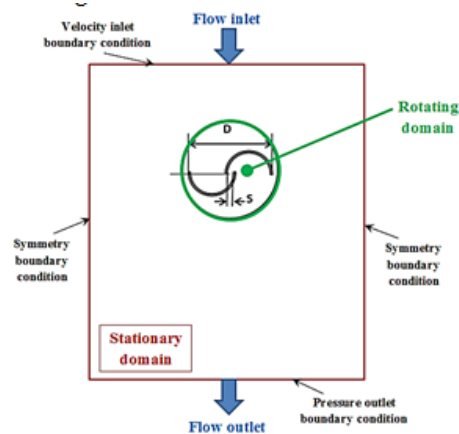


FIG 5. Computational domain

The stationary zone takes the form of a rectangle with dimensions matching the dimensions of the wind tunnel test section described by Roy and Saha [14]. The inlet and outlet boundary conditions of the computational grid are described as velocity inlet and pressure outlet, respectively. The other sides of the rectangular domain are symmetric boundaries. Five values of the inlet velocity were used in the current study; 6, 7, 8, 9, and 10 m/s. The atmospheric pressure value was set at the outlet domain boundary.

### 3.6 Grid Sensitivity Analysis

The solution accuracy is related to the number of control volumes inside the computational zone. As the number of mesh cells increases, the accuracy of the solution increases but the computational time increases as well. Consequently, there is a necessity of having a specific mesh distribution that will satisfy the requirements of high solution accuracy with less computational time. Grid independence analysis was performed in order to get the minimum number of mesh elements, which does not influence the examined parameter results. Torque coefficient was selected as the examined parameter. Grid refinements were carried out until the torque coefficient becomes steady. This test was performed corresponding to tip-speed ratio of 0.38377. Figure 6 shows the variation of the torque coefficient with the number of mesh cells. It may be noted that the torque coefficient becomes steady when the number of mesh elements is higher than 132000. The final selected mesh for the current study contains 155887 elements.

No. of cells	$C_T$
40168	0.4
60257	0.385
80133	0.38
101860	0.3755
131891	0.3719
155887	0.3718
171475	0.3714

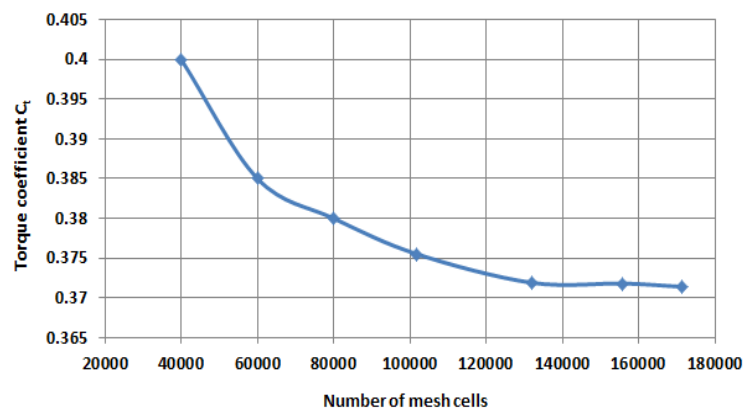


FIG 6. Grid independence test results at tip speed ratio = 0.38377

### 3.7 Validation

For the purpose of ensuring the accuracy of the CFD model, results extracted from the CFD model were compared to the experimental results presented by Irbu and Roy [25] as shown in Fig.7. The torque coefficient variation with the tip speed ratio resulted from the CFD model is in a good agreement with the results of the experimental study [25].

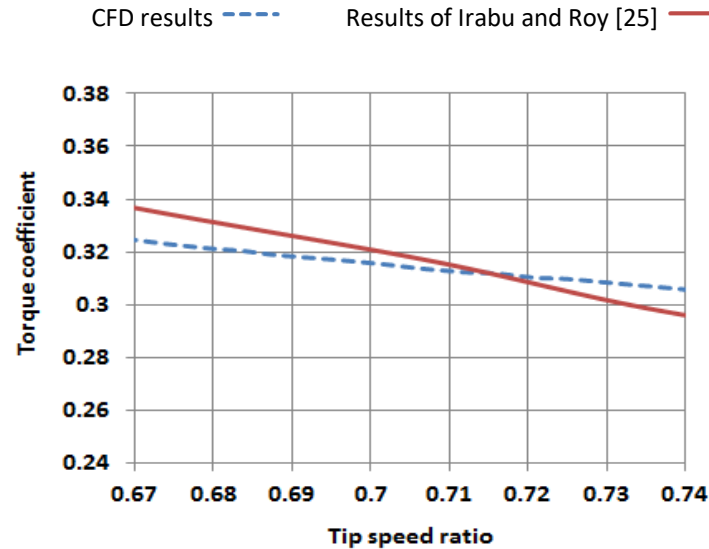
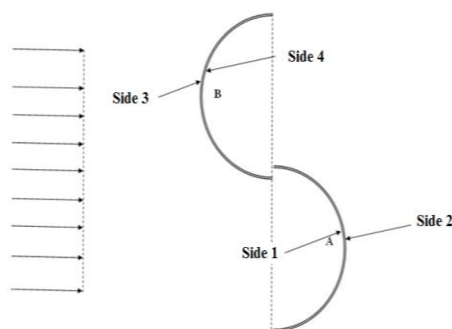


FIG 7. Torque coefficient variation with tip speed ratio for the CFD results and for the results of Irbu and Roy [25]

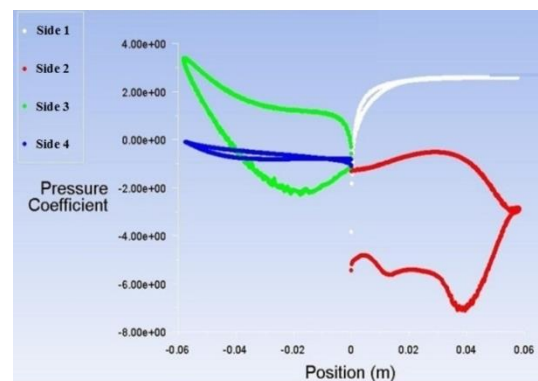
## 4. RESULTS

### 4.1 Performance of the Savonius Turbine with Conventional Semi-circle Blades Design

In order to study the behaviour of the Savonius wind turbine, qualitative analysis of pressure and velocity contours was applied. Moreover, the pressure coefficient is plotted on the turbine blades at different angles of rotation to show the contribution of drag forces to the torque production mechanism as shown in Fig 8, 9, and 10. At  $\theta = 0^\circ$  (Fig.8), the stagnation point was formed nearly at the middle of the returning bucket (bucket B) because of the high values of the relative velocities of the resisting flow that stagnated at that point. The advanced bucket (bucket A) produces positive torque while the returning bucket produces a resisting torque with a larger value leading to net torque with a negative value. At  $\theta = 16^\circ$  (Fig.9), the resisting flow will start to decrease when the wind turbine starts to rotate, and returning bucket advances in motion as the blockage projected area starts to decrease. The stagnation point starts to move outwards on bucket B when it advances in motion until the stagnation point diminishes meanwhile, another stagnation point is developing on bucket A that became now the returning bucket. At  $\theta = 110^\circ$  (Fig.10), low pressure area appears behind the bucket A, and expands gradually with the increase of the angle of rotation.



(a) Schematic diagram showing configuration



(b) Pressure coefficient

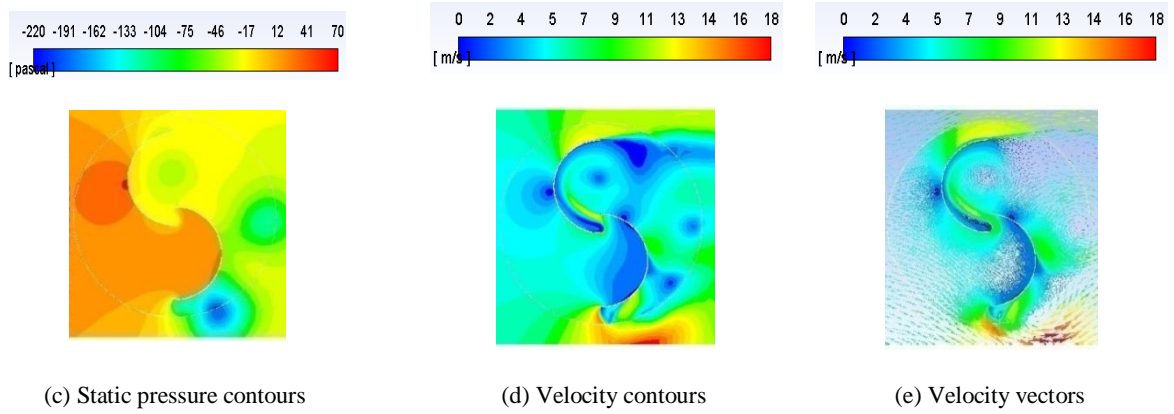


FIG 8. Pressure coefficient, static pressure contours, velocity contours, and velocity vectors and at  $\theta = 0^\circ$

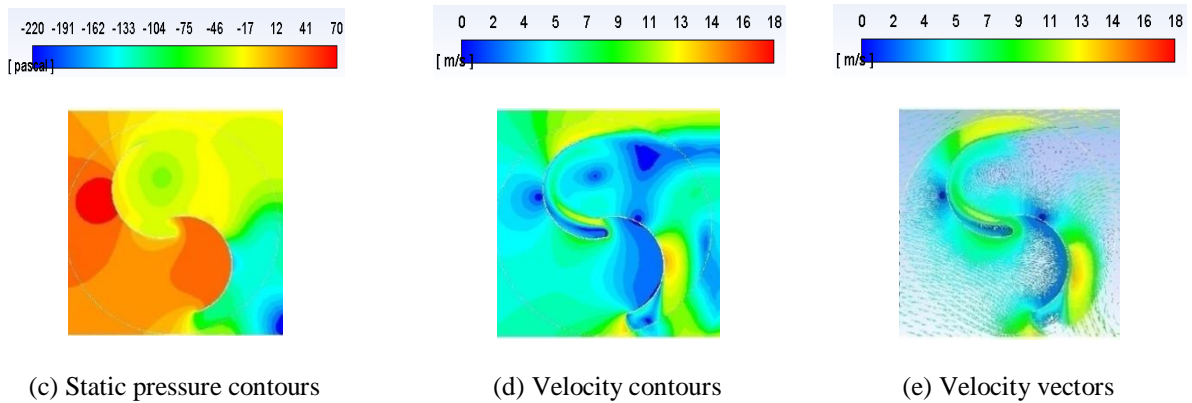
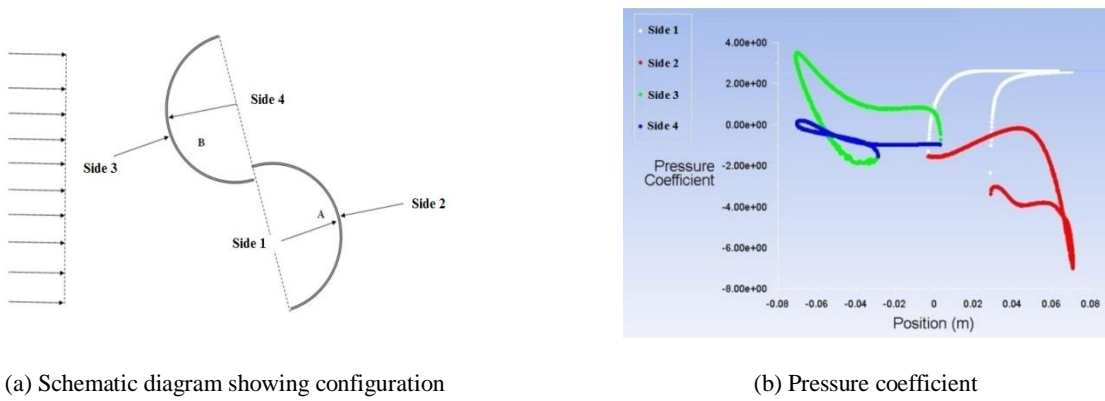
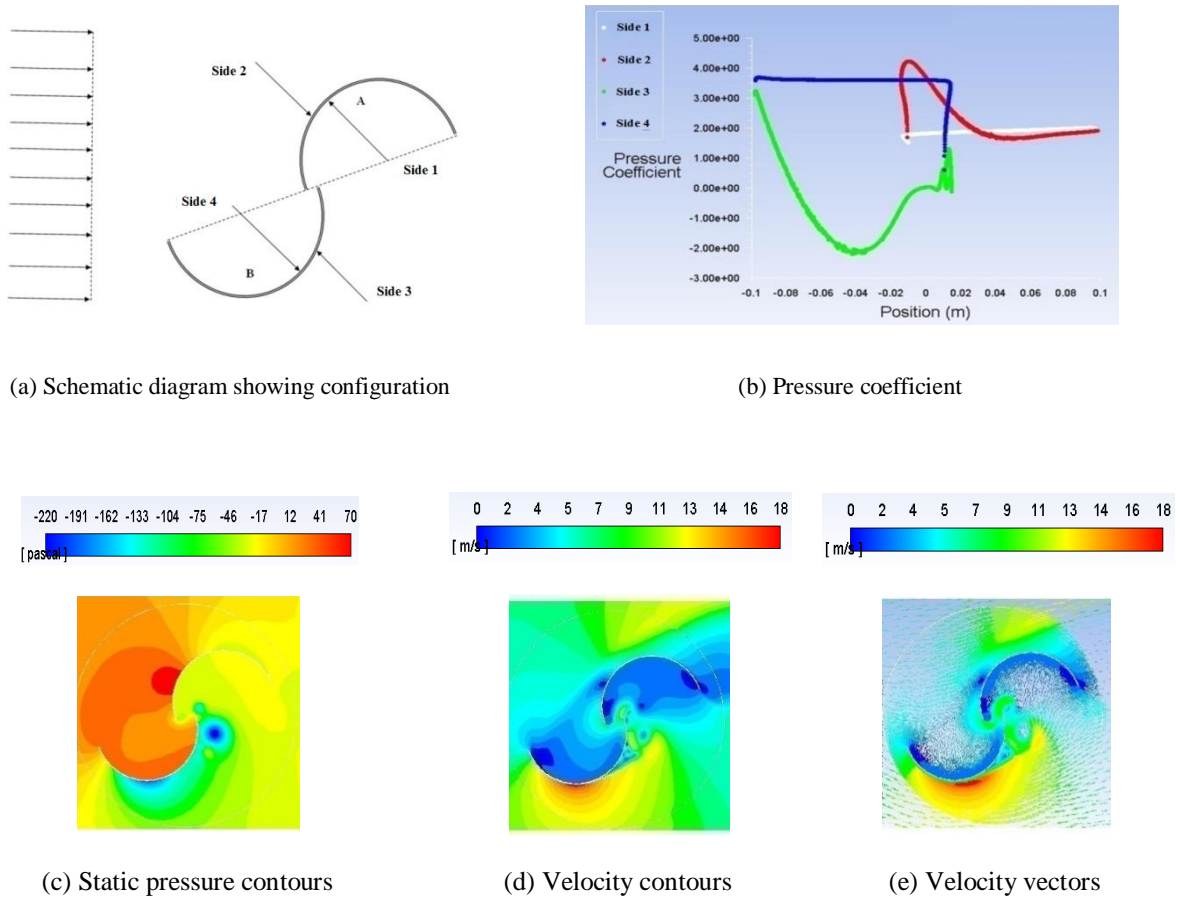


FIG 9. Pressure coefficient, static pressure contours, velocity contours, and velocity vectors and at  $\theta = 16^\circ$



(a) Schematic diagram showing configuration

(b) Pressure coefficient

[ -220 -191 -162 -133 -104 -75 -46 -17 12 41 70 ]  
[ pascal ]

[ 0 2 4 5 7 9 11 13 14 16 18 ]  
[ m/s ]

[ 0 2 4 5 7 9 11 13 14 16 18 ]  
[ m/s ]

(c) Static pressure contours

(d) Velocity contours

(e) Velocity vectors

**FIG 10. Pressure coefficient, static pressure contours, velocity contours, and velocity vectors and at  $\theta = 110^\circ$**

**4.2. New Suggested Savonius Turbine Designs Based on Modification of Blades Profile**

A complete converged solution of a numerical simulation of the Savonius turbine with semi-circular blades was used as an initial solution for the optimization analysis. Using the Adjoint method, and by setting the objective to be torque optimization, the semi-circle blade shape was modified. There are two different profiles shape resulted from the optimization process profile 1 and profile 2 as shown in Fig. 11.

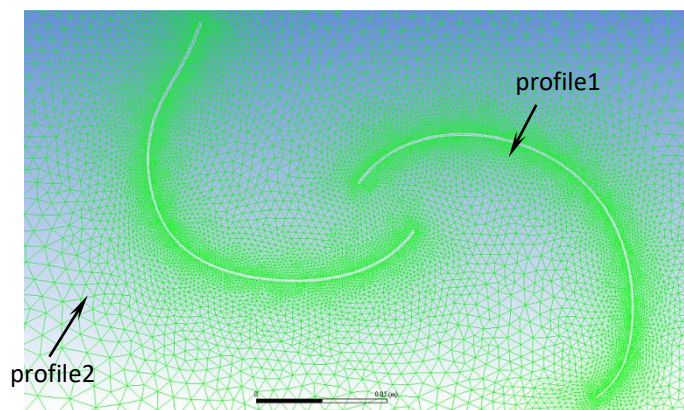


**FIG 11. Shape of blades at the end of the optimization process**

Practically, when using non-similar blades, this may lead to instability issues during the rotation of the turbine. Based on that, three designs were proposed as indicated in table 1 in a way to make the two blades similar for each design and in the meantime using the generated profiles from the optimization analysis.

**TABLE 1. Description of blade profile used for each proposed design**

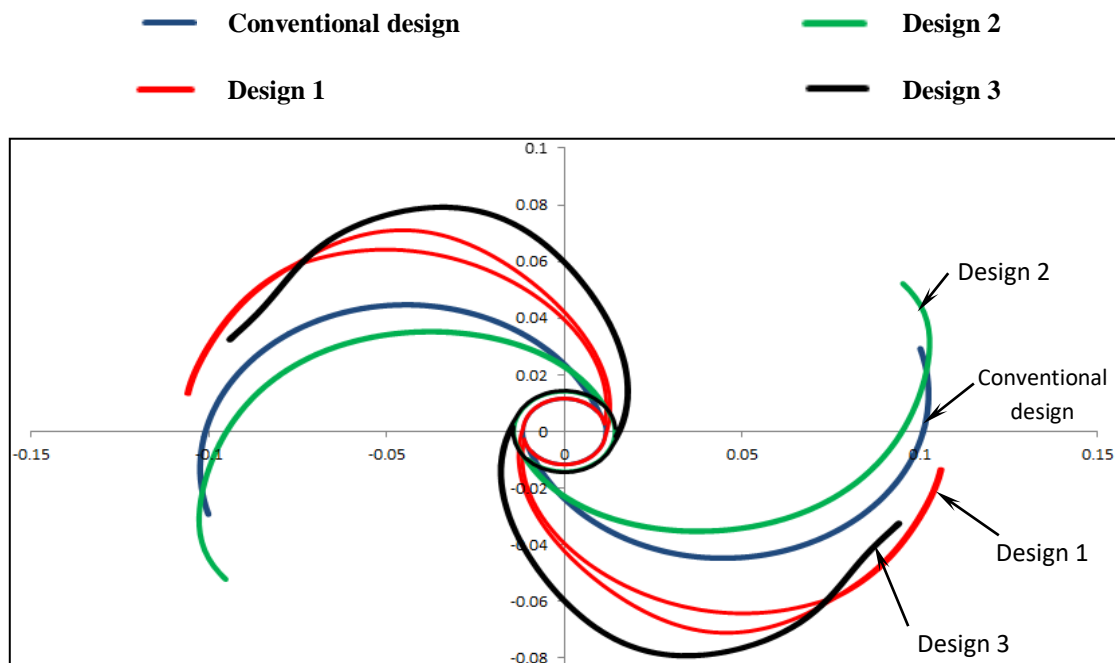
Proposed design name	Blade profile used for the two blades
Design 1	Combination of profiles 1, 2, and conventional semi-circle profile
Design 2	Profile 1
Design 3	Profile 2

The idea of the three suggested designs is to test each profile coming out from the optimization simulation separately in addition to test the effect of combining them with the conventional shape. Design 1 was proposed to be based on combining the blade profiles 1, and 2 with the conventional semi-circle profile. Designs 2 and 3 were suggested to use profiles 1 and 2 respectively.

The profile of blades for the three proposed designs and for the conventional semi-circle design are presented in Fig. 12.

#### 4.3 Performance of the New Suggested Designs of the Savonius Wind Turbine

Numerical simulations were conducted at five different free stream wind speeds (6, 7, 8, 9, and 10 m/s) for the conventional semi-circle design and also for design 1, 2, and 3. The following sections present detailed comparisons between these cases.

**FIGURE 12. Shape of blades for the conventional design and for designs 1, 2, and 3**

##### 4.3.1 Pressure distribution at different free stream wind speeds

Figure 13 shows pressure distribution for the new suggested designs and for the conventional semi-circle design at three different free stream wind speeds (6, 8, and 10 m/s).

By comparing the pressure contours for all designs at the same velocity of 6 m/s, the following conclusions can be drawn:

- There is a small region with rotating vortices appearing at the tip of the lower blade for all designs except for design 3. These vortices are formed due to the interaction between the free wind steam and the flow pushed by the blade rotation. For design 3, the trajectory of interaction shown in Fig. 13 is deviated toward the lower blade compared to other designs, and this minimized the chance of vortices formation.

- Due to having a specific blade profile in design 3 so that the blade profile is directed inward gradually and then switched to the outward direction slightly; the separation point is delayed compared to other designs.
- The pressure difference between surfaces of each blade in design 3 is relatively high when comparing with other designs. The reason for that is the high pressure side of the blade in design 3 is expanded to involve additional surface area due to the shift of the separation point.

Increasing the free stream wind speed from 6 to 8 and also to 10 m/s, results in having higher values of pressure at the stagnation regions. The expansion of high pressure zone away from the rotating zone is recognized. Design 3 keeps the same strength points mentioned earlier relative to other designs at speeds higher than 6 m/s.

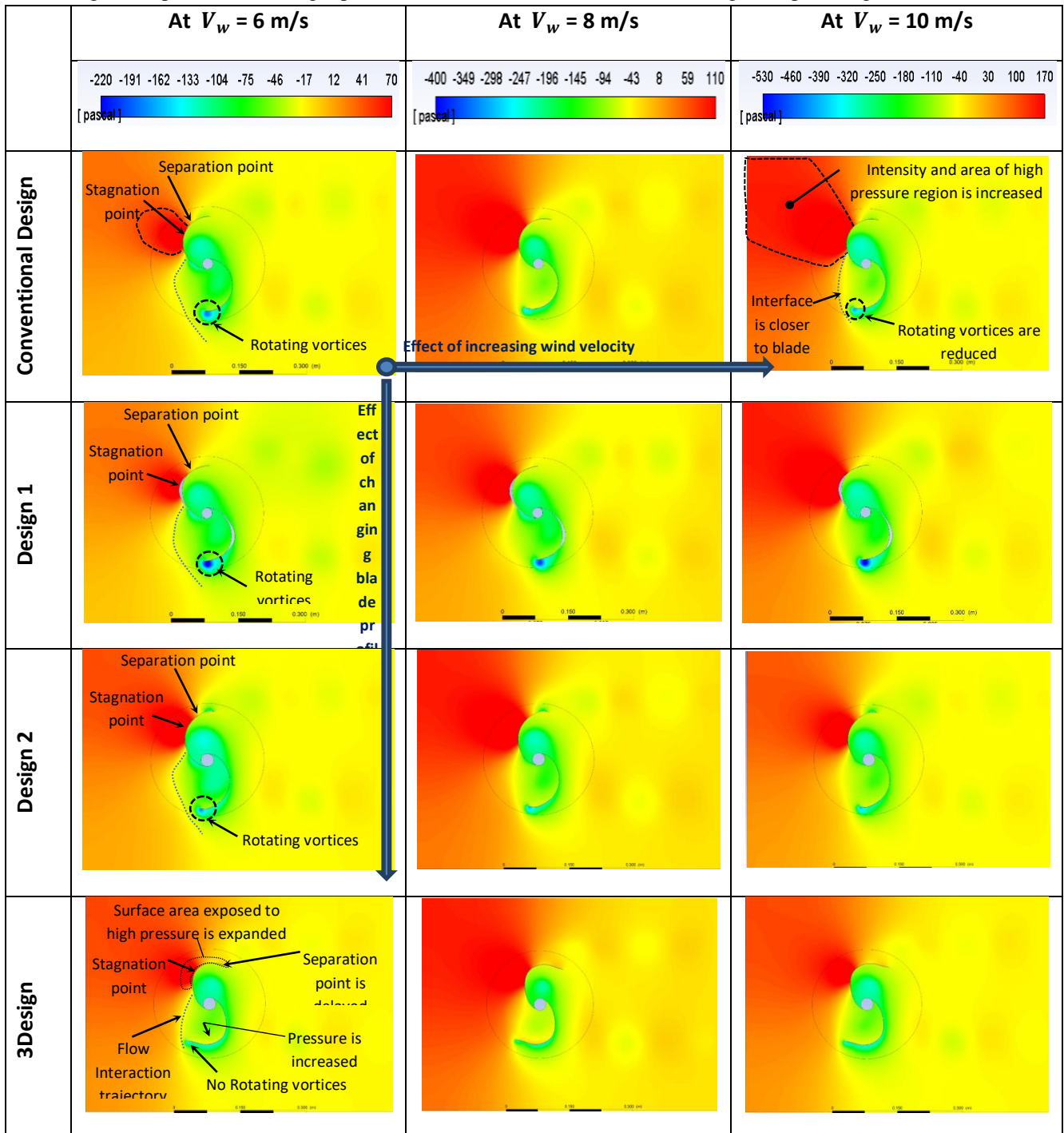


FIG 13. Pressure contours for various turbine designs at  $V_w = 6, 8,$  and  $10$  m/s

**4.3.2 Velocity distribution at different free stream wind speeds**

Figure 14 shows velocity distribution for the new suggested designs and for the conventional semi-circle design at three different free stream wind speeds (6, 8, and 10 m/s). The velocity contours shown in Fig. 14 demonstrate the low velocity zone formed behind the blade and the low velocity area at the stagnation point for each case.

It may be noted that for design 3, there is a secondary stagnation zone structure formed close to the main stagnation zone. The reason for the formation of this secondary stagnation zone is that the optimized blade profile in design 3 has a slight and gradual outward curvature close to the blade tip region instead of moving inward like for the semi-circle blade design resulting in extension of the interaction with incoming flow and delaying separation.

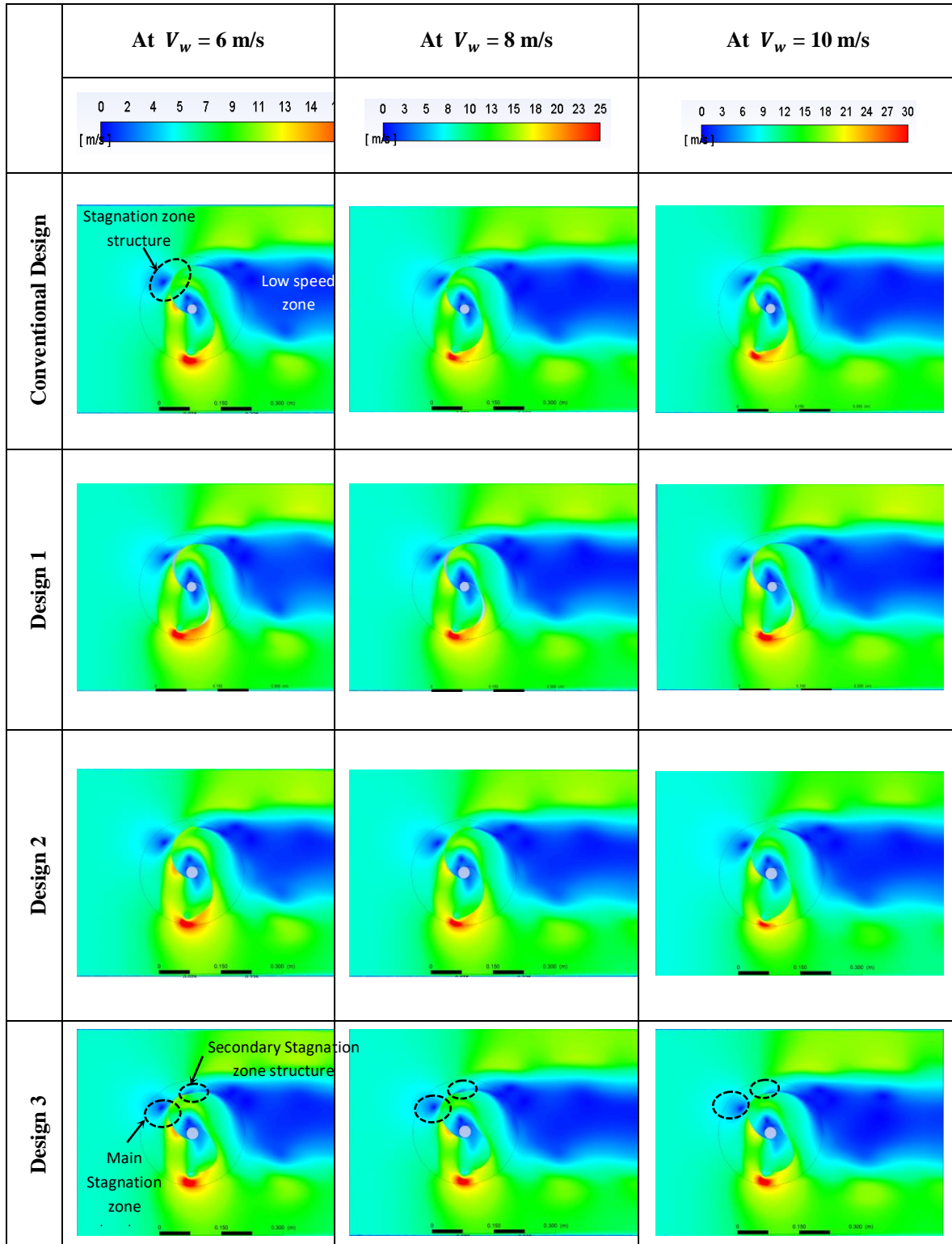


FIG 14. Velocity contours for various turbine designs at  $V_w = 6, 8,$  and  $10$  m/s

4.3.3 Tip speed ratio, torque coefficient, and power coefficient at various free stream wind speeds

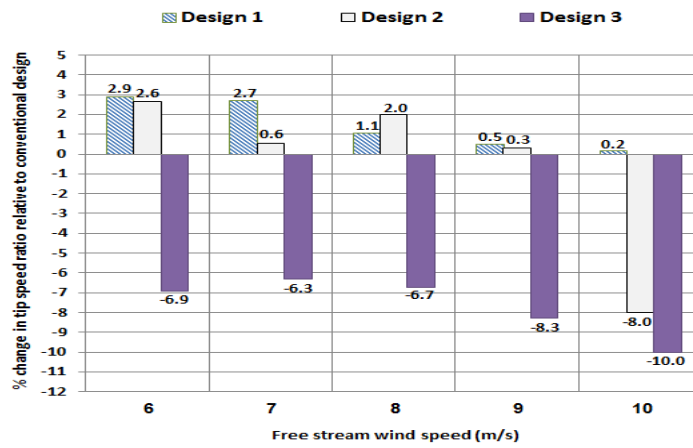


FIG 15. Percentage change in tip speed ratio for designs 1, 2, and 3 with respect to the conventional design at different values of  $V_w$

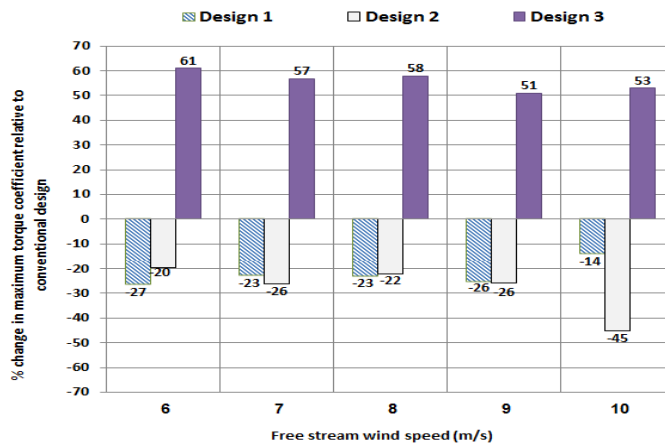


FIG16. Percentage change in maximum torque coefficients for designs 1, 2, and 3 with respect to the conventional design at different values of  $V_w$

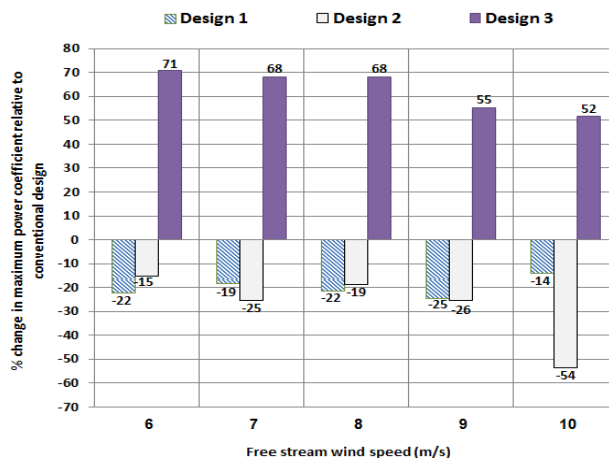


FIG 17. Percentage change in maximum power coefficients for designs 1, 2, and 3 with respect to the conventional design at different values of  $V_w$

Figures 15, 16, and 17 show the percentage increase of tip speed ratio, torque coefficient, and power coefficient respectively for the new suggested designs compared to the conventional design at five different free stream wind speeds.

It may be noted from Fig. 17 that design 3 provided significant increase in  $C_p$  compared to the conventional semi-circle design and other designs especially at lower values of  $V_w$ . The maximum % increase in  $C_p$  is 71% corresponding to  $V_w = 6$  m/s for design 3, while the minimum % increase in  $C_p$  is 52% corresponding to  $V_w = 10$  m/s.

On the contrary, designs 1 and 2 do not provide any increase in  $C_p$  compared to the conventional semi-circle design at all values of  $V_w$  as can be seen from Fig.17.

The results presented in Fig. 17 is connected to the data shown in Fig. 15 and Fig. 16, because  $C_p$  depends on both of  $\lambda$  and  $C_T$  as discussed earlier regarding equation 17, so the % variation in  $C_p$  can be analyzed by knowing the % variation in  $\lambda$  and  $C_T$ . Based on that, it may be concluded that design 3 achieves significant improvement of  $C_T$  with values higher than 51% (Fig.16) with respect to the conventional design but with corresponding slight drop in the values of  $\lambda$  with values less than 10% (Fig.15).

As shown in Fig.17, improvement of  $C_p$  with at least 52% with respect to the conventional design is notable with design 3. This could be attributed to the combined effect of the changes in  $\lambda$  and  $C_T$  results in.

The most effective factor in the deterioration of the performance of design 1 and design 2 compared to the conventional design is that the suggested blade profiles failed in delaying the flow separation and minimizing wake flow at blades tip. On the other hand, the blades profile of design 3 delayed the separation point and allowed better pressure distribution on blades surfaces resulted in higher force and consequently higher torque.

## 5. CONCLUSIONS

Simple changes in the blade profile of Savonius wind turbines may lead to significant changes in the pressure distribution, then the torque and power generated. The optimal control approach was used to find the best possible blade profile that will optimize the power coefficient. In the light of the obtained results, the following conclusions can be drawn:

- Proposed design 3 provided significant increase in the power coefficient compared to the conventional semi-circle design and proposed designs 1 & 2. The maximum increase in  $C_p$  for design 3 compared to the semi-circle design is 71% corresponding to  $V_w = 6$  m/s, while the minimum % increase in  $C_p$  is 52% corresponding to  $V_w = 10$  m/s.
- Analysis of the blade profile of the proposed design 3 refers to that the most critical part of the blade that leads to changes in the performance is the second half of the blade close to the tip. Modification of this part so that the blade profile is directed inward gradually and then switched to the outward direction slightly, increases the efficiency of the turbine as it achieves the following:
  - Delay of the flow separation point to be close to the tip.
  - Increasing of the blade surface area subjected to high pressure due to the expansion of the stagnation zone.
  - Minimization of the rotating vortices at the tip of blades by shifting the interface between the incoming flow and the flow pushed by the blade.

## REFERENCES

- [1] R. Kumar, K. Raahemifar, and A. S. Fung, "A critical review of vertical axis wind turbines for urban applications," *Renewable and Sustainable Energy Reviews* 89, 2018, pp. 281-291.
- [2] S. S. Johannes, 1929, "Rotor adapted to be driven by wind or flowing water," Google Patents.
- [3] J. V. Akwa, H. A. Vielmo, and A. P. Petry, "A review on the performance of Savonius wind turbines," *Renewable and sustainable energy reviews* 16(5), 2012, pp. 3054-3064.
- [4] R. Hassanzadeh, M. Mohammadnejad, and S. Mostafavi, "Comparison of various blade profiles in a two-blade conventional Savonius wind turbine," *Journal of Energy Resources Technology* 143(2), 2020.
- [5] U. Saha, S. Thotla, and D. Maity, "Optimum design configuration of Savonius rotor through wind tunnel experiments," *Journal of Wind Engineering and Industrial Aerodynamics*, 96(8-9), 2008, pp. 1359-1375.
- [6] M. Kamoji, S. Kedare, and S. Prabhu, "Performance tests on helical Savonius rotors," *Renewable Energy*, 34(3), 2009, pp. 521-529.
- [7] J.-H. Lee, Y.-T. Lee, and H.-C. Lim, "Effect of twist angle on the performance of Savonius wind turbine," *Renewable Energy*, 89, 2016, pp. 231-244.
- [8] W. El-Askary, A. S. Saad, A. M. AbdelSalam, and I. Sakr, "Experimental and theoretical studies for improving the performance of a modified shape

- Savonius wind turbine," *Journal of Energy Resources Technology*, 142(12), 2020.
- [9] B. Zhang, B. Song, Z. Mao, and W. Tian, "A novel wake energy reuse method to optimize the layout for Savonius-type vertical axis wind turbines," *Energy*, 121, 2017, pp. 341-355.
- [10] H. Gad, A. Abd El-Hamid, W. El-Askary, and M. Nasef, "A New design of Savonius wind turbine: numerical study," *CFD Letters*, 6(4), 2014, pp. 144-158.
- [11] N. Alom, and U. K. Saha, "Examining the aerodynamic drag and lift characteristics of a newly developed elliptical-bladed Savonius rotor," *Journal of Energy Resources Technology*, 141(5), 2019.
- [12] K. Kacprzak, G. Liskiewicz, and K. Sobczak, "Numerical investigation of conventional and modified Savonius wind turbines," *Renewable energy*, 60, 2013, pp. 578-585.
- [13] N. Alom, and U. K. Saha, "Influence of blade profiles on Savonius rotor performance: Numerical simulation and experimental validation," *Energy Conversion and Management*, 186, 2019, pp. 267-277.
- [14] S. Roy, and U. K. Saha, "Wind tunnel experiments of a newly developed two-bladed Savonius-style wind turbine," *Applied Energy*, 137, 2015, pp. 117-125.
- [15] S. Roy, and A. Ducoin, "Unsteady analysis on the instantaneous forces and moment arms acting on a novel Savonius-style wind turbine," *Energy Conversion and Management*, 121, 2016, pp. 281-296.
- [16] A. Ramadan, K. Yousef, M. Said, and M. Mohamed, "Shape optimization and experimental validation of a drag vertical axis wind turbine," *Energy*, 151, 2018, pp. 839-853.
- [17] M. Tartuferi, V. D'Alessandro, S. Montelpare, and R. Ricci, "Enhancement of Savonius wind rotor aerodynamic performance: a computational study of new blade shapes and curtain systems," *Energy*, 79, 2015, pp. 371-384.
- [18] W. Tian, Z. Mao, B. Zhang, and Y. Li, "Shape optimization of a Savonius wind rotor with different convex and concave sides," *Renewable energy*, 117, 2018, pp. 287-299.
- [19] U. H. Rathod, P. K. Talukdar, V. Kulkarni, and U. K. Saha, "Effect of Capped Vents on Torque Distribution of a Semicircular-Bladed Savonius Wind Rotor," *Journal of Energy Resources Technology*, 141(10), 2019.
- [20] A. Roshan, A. Sagharichi, and M. J. Maghrebi, "Nondimensional Parameters' Effects on Hybrid Darrieus-Savonius Wind Turbine Performance," *Journal of Energy Resources Technology*, 142(1), 2020.
- [21] H. A. H. Saeed, A. M. N. Elmekawy, and S. Z. Kassab, "Numerical study of improving Savonius turbine power coefficient by various blade shapes," *Alexandria Engineering Journal*, 58(2), 2019, pp. 429-441.
- [22] Ansys Fluent Adjoint Solver, ANSYS, Inc. Release 15.0 Southpointe, 2013, 275 Technology Drive, Canonsburg, PA 15317, ansysinfo@ansys.com, <http://www.ansys.com>
- [23] T. Han, S. Kaushik, R. Gin, and E. Bot, 2012, "Adjoint Method for Aerodynamic Shape Improvement," No. 0148-7191, SAE Technical Paper.
- [24] M. W. Bern, and P. E. Plassmann, "Mesh Generation," *Handbook of computational geometry*, 38, 2000.
- K. Irabu, and J. N. Roy, "Characteristics of wind power on Savonius rotor using a guide-box tunnel," *Experimental thermal and fluid science*, 32(2), 2007, pp. 580-586.